A Systematic Electromagnetic-Circuit Method for EMI Analysis of Coupled Interconnects on Dispersive Dielectrics

Min Tang, *Member, IEEE*, Jiaqing Lu, Junfa Mao, *Fellow, IEEE*, and Lijun Jiang, *Member, IEEE*

***Abstract*—This paper presents a systematic electromagnetic-circuit method for efficient simulation of coupled interconnects on dispersive dielectrics in the presence of electromagnetic interference. The dispersive substrate of coupled interconnects is characterized by the multiterm Debye or Lorentz formula. According to the differential equations derived from the equivalent circuit modeling of dispersive media, the full-wave finite-difference time-domain algorithm is utilized to capture accurate field in a dispersive substrate. The effects of incident field, under the quasi-TEM assumption, are then represented by the distributed sources along transmission lines. An efficient algorithm based on the waveform relaxation with transverse partitioning (WR-TP) is employed for fast simulation of coupled transmission lines. A simple and clear derivation of the relaxation sources in WR-TP is described and the compact results are given. The impact of dispersive dielectrics on the incident field, and thus to the transient response of interconnects, is investigated by comparison with conventional techniques. Several numerical examples are given to illustrate the accuracy and efficiency of the proposed method.**

***Index Terms*—Electromagnetic interference (EMI), finite difference time domain (FDTD), frequency-dependent parameters, interconnects, waveform relaxation.**

I. Introduction

With the ever-increasing operating speeds and decreasing structure sizes, electromagnetic compatibility (EMC) has become a major concern in modern circuit designs since high-speed interconnects at various hierarchical levels may serve as spurious antennas at high frequencies and lead to strong coupling of electromagnetic interference (EMI). This electromagnetic coupling can seriously deteriorate the signal integrity of the design and cause false switching of waveforms. Meanwhile, due to skin, edge, and proximity effects and lossy substrates, the frequency dependence of interconnect parameters becomes more and more popular in practical cases [1]. Successful modeling of interconnects requires accurate material parameter characterization over a wide band of frequencies. For example, wideband frequency-domain characterization of FR-4 has been described in [2] and [3], where the real and imaginary parts of the complex permittivity were related by the Hilbert transform, a causal response in the time domain was obtained thereby. In [4], the partial-element equivalent-circuit (PEEC) modeling of dispersive dielectrics was introduced, where the general media are represented by the Debye, as well as Lorentz, models and its validity was illustrated by different transmission-line structures.

Incorporating the effects of incident electromagnetic fields into interconnect simulation has been a problem of interest for many years. The most general approach to solve this problem is the full-wave technique formulated as the 3-D electromagnetic field. While accurate, this kind of algorithm would require great computational resources if applied to practical sized printed circuit board (PCB) problems. Thus, for many practical cases, it is more common to use the distributed transmission-line model under the quasi-TEM assumption, where the existence of external field coupling is introduced by distributed voltage and current sources along the lines [5], [6]. Various techniques have been proposed for solving the transmission-line model with distributed sources [5]–[15]. To guarantee the passivity in the developed model, an algorithm based on the matrix rational approximation (MRA) [16] has been presented for macromodeling of transmission lines. By employing the delay extraction technique, this method can also deal with long delay transmission lines in the presence of EMI [13]. Recently, a new spectral formulation has also been presented for the transient analysis of plane-wave coupling to transmission lines with frequency-dependent parameters [15]. Nevertheless, most of these techniques treat the medium surrounding interconnects as homogenous air in the calculation of incident field. Despite its simplicity, imposing such a condition may produce poor results at high frequencies. In [11], an efficient physical optics technique has been utilized to calculated the field in a layered inhomogeneous medium. In [12], a full-wave field simulation has been carried out to accurately characterize the perturbation of the incident field due to the dielectric substrate. The dispersion of substrate material, however, was not taken into consideration.

For EMI analysis, another challenge is that of the large number of coupled lines in an interconnection structure. In recent years, an efficient method based on waveform relaxation with transverse partitioning (WR-TP) [17] was presented for the simulation of large coupled interconnects. In WR-TP, the coupling effects due to the neighboring lines are represented by

Manuscript received May 16, 2012; accepted August 28, 2012. Date of publication October 18, 2012; date of current version January 17, 2013. This work was supported in part by the National Science Foundation of China under Grant 60906016 and in part by the National Basic Research Program of China under Grant 2009CB320202.

M. Tang, J. Lu, and J. Mao are with the Key Laboratory of Ministry of Education of China for Research of Design and Electromagnetic Compatibility of High Speed Electronic Systems, Shanghai Jiao Tong University, Shanghai 200240, China (e-mail: tm222@sjtu.edu.cn; jfmao@sjtu.edu.cn).

L. Jiang is with the Department of Electrical and Electronic Engineering, University of Hong Kong, Kowloon, Hong Kong (e-mail: ljiang@eee.hku.hk).

Color versions of one or more of the figures in this paper are available online at http://ieeexplore.ieee.org.

Digital Object Identifier 10.1109/TMTT.2012.2220562

the relaxation voltage and current sources within the sub-circuits. The computational cost of this algorithm grows almost linearly with the number of coupled lines, providing a significant speedup compared to conventional model. It is also highly suitable for parallel implementation for further improvement of efficiency. In the past few years, this WR-TP technique has been extended to the simulation of coupled interconnects with frequency-dependent parameters [18]. More recently, a parallel algorithm based on the physical and time-domain partitioning has been proposed for simulations of massively coupled interconnects [19]. The WR-TP algorithm has also been implemented for fast simulation of interconnects in the presence of incident field [14]. Nevertheless, the impact of the dielectric substrate on the incident field was ignored in the calculation, which would cause incorrect transient response along the transmission lines.

In this paper, an efficient hybrid method for EMI analysis of coupled interconnects on dispersive dielectrics is presented. The implementation of this method consists of two stages, one is for electromagnetic simulation and the other is for circuit simulation. In the electromagnetic simulation, in order to accurately model the field in a dispersive substrate, a full-wave finite-difference time-domain (FDTD) algorithm is exploited based on the differential equations derived from the equivalent circuit modeling (ECM) technique. Both the Debye and Lorentz media are taken into consideration in the modeling. In the region of circuit simulation, the WR-TP approach is utilized for efficient computation of coupled transmission lines with frequency-dependent parameters in the presence of EMI. The relaxation voltage and current sources in the algorithm are derived and described in a compact form. Additional distributed voltage sources, which denote the effects of the excitation field, are computed with the results obtained from the electromagnetic simulation.

This paper is organized as follows. In Section II, the modeling of transmission lines with frequency-dependent parameters and incident field coupling is described. In Section III, the WR-TP algorithm is employed for efficient EMI simulation of coupled interconnects. In Section IV, full-wave electromagnetic simulation of the incident field in the dispersive media is proposed. The numerical results and conclusion are presented in Sections V and VI, respectively

II. Modeling of Interconnects With Frequency-Dependent Parameters and Incident Field Coupling

A. Formulation of Transmission Lines for EMI Analysis

Consider N-coupled transmission lines excited by an incident electromagnetic field, as shown in Fig. 1.

Depending on the definition of line voltage, two different, but equivalent formulations can be derived to describe transmission lines [6]. The transmission-line equations in terms of total voltages are given by

$$\frac{d\boldsymbol{V}(z,s)}{dz}+\boldsymbol{Z}(s)\boldsymbol{I}(z,s)=\boldsymbol{V}_F(z,s) \tag{1a}$$

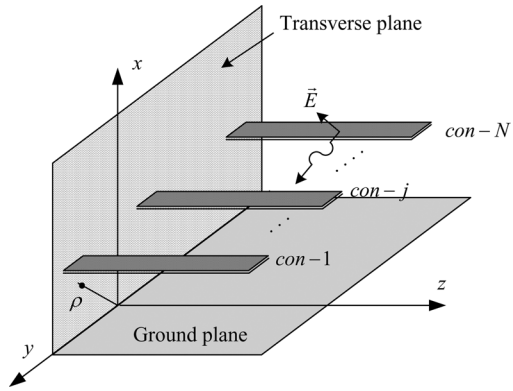

Fig. 1. Geometry of interconnects with incident field coupling (the substrate is not depicted for clarity).

$$\frac{d\boldsymbol{I}(z,s)}{dz}+\boldsymbol{Y}(s)\boldsymbol{V}(z,s)=\boldsymbol{I}_F(z,s) \tag{1b}$$

where

$$\boldsymbol{V}_F(z,s)=\boldsymbol{F}(z,s)-\begin{bmatrix}\vdots\\ \frac{d}{dz}\int_{\rho^j(x,y)}E_t(\rho,z,s)d\rho\\ \vdots\end{bmatrix} \tag{1c}$$

$$\boldsymbol{I}_F(z,s)=-\boldsymbol{Y}(s)\begin{bmatrix}\vdots\\ \int_{\rho^j(x,y)}E_t(\rho,z,s)d\rho\\ \vdots\end{bmatrix}. \tag{1d}$$

In $\boldsymbol{V}_F(z,s)$, $\boldsymbol{F}(z,s)$ is expressed as

$$\boldsymbol{F}(z,s)=\begin{bmatrix}\vdots\\ E_z(\mathrm{con}\_k,z,s)-E_z(\mathrm{ref},z,s)\\ \vdots\end{bmatrix} \tag{1e}$$

where E_z is the axial component of the incident field, E_t is the transverse component of the incident field, con_k denotes the kth conductor, and ρ is a contour in the transverse (x,y) plane.

From (1a)–(1e), it is easy to derive the transmission-line equations in terms of scattered voltages as

$$\frac{d\boldsymbol{V}^s(z,s)}{dz}+\boldsymbol{Z}(s)\boldsymbol{I}(z,s)=\boldsymbol{F}(z,s) \tag{2a}$$

$$\frac{d\boldsymbol{I}(z,s)}{dz}+\boldsymbol{Y}(s)\boldsymbol{V}^s(z,s)=\boldsymbol{0}. \tag{2b}$$

The scattered voltage $\boldsymbol{V}^s$ along the transmission lines is related to the total voltage $\boldsymbol{V}$ by the following expression [6]:

$$\boldsymbol{V}(z,s)=\boldsymbol{V}^s(z,s)+\boldsymbol{T}(z,s) \tag{3a}$$

where

$$\boldsymbol{T}(z,s)=-\begin{bmatrix}\vdots\\ \int_{\rho^j(x,y)}E_t(\rho,z,s)d\rho\\ \vdots\end{bmatrix}. \tag{3b}$$

By comparison, the transmission-line equations in terms of scattered voltages are more convenient to deal with lines with frequency-dependent parameters since there is not distributed current source in (2b). Therefore, the following derivations are all based on the expressions of (2a) and (2b). For convenience, however, the superscript s on the scattered voltage $\boldsymbol{V}^s$ will be suppressed.

B. Modeling of Transmission Lines With Frequency-Dependent Parameters

Without loss of generality, it is assumed that the per-unit-length (p.u.l.) frequency-dependent parameters of transmission lines are obtained at a set of discrete frequencies. The vector-fitting algorithm [20] followed by a passive check and compensation technique [21] is used to generate the positive-real closed form of the series impedance matrix and parallel admittance matrix

$$\boldsymbol{Z}(s) \cong \boldsymbol{R}_0 + s\boldsymbol{L}_0 + \sum_{q=1}^{Q_1} \frac{1}{s - P_q}\boldsymbol{R}_q \tag{4a}$$

$$\boldsymbol{Y}(s) \cong \boldsymbol{G}_0 + s\boldsymbol{C}_0 + \sum_{q=1}^{Q_2} \frac{1}{s - B_q}\boldsymbol{G}_q \tag{4b}$$

where Q_1 and Q_2 represent the number of poles used in the rational approximation. These equations can be cast into the realizable form of an equivalent circuit network as [22]

$$\boldsymbol{Z}(s) = \bar{\boldsymbol{R}}_0 + s\boldsymbol{L}_0 + \sum_{q=1}^{Q_1} \frac{s}{s - P_q}\bar{\boldsymbol{R}}_q \tag{5a}$$

$$\boldsymbol{Y}(s) = \bar{\boldsymbol{G}}_0 + s\boldsymbol{C}_0 + \sum_{q=1}^{Q_2} \frac{s}{s - B_q}\bar{\boldsymbol{G}}_q \tag{5b}$$

where $\bar{\boldsymbol{R}}_0$ and $\bar{\boldsymbol{R}}_q$ are the equivalent resistance, $\bar{\boldsymbol{G}}_0$ and $\bar{\boldsymbol{G}}_q$ are the equivalent conductance, and are given by

$$\bar{\boldsymbol{R}}_0 = \boldsymbol{R}_0 - \sum_{q=1}^{Q_1} \frac{1}{P_q}\boldsymbol{R}_q \tag{5c}$$

$$\bar{\boldsymbol{R}}_q = \frac{1}{P_q}\boldsymbol{R}_q \tag{5d}$$

$$\bar{\boldsymbol{G}}_0 = \boldsymbol{G}_0 - \sum_{q=1}^{Q_2} \frac{1}{B_q}\boldsymbol{G}_q \tag{5e}$$

$$\bar{\boldsymbol{G}}_q = \frac{1}{B_q}\boldsymbol{G}_q. \tag{5f}$$

The generalized equivalent circuit representations [23] of series impedance matrix $\boldsymbol{Z}(s)$ and parallel admittance matrix $\boldsymbol{Y}(s)$ are described in Fig. 2. The equivalent inductance $\bar{\boldsymbol{L}}_q$ and equivalent capacitance $\bar{\boldsymbol{C}}_q$ in Fig. 2 are given, respectively, by

$$\bar{\boldsymbol{L}}_q = -\frac{1}{P_q}\bar{\boldsymbol{R}}_q \tag{6a}$$

and

$$\bar{\boldsymbol{C}}_q = -\frac{1}{B_q}\bar{\boldsymbol{G}}_q. \tag{6b}$$

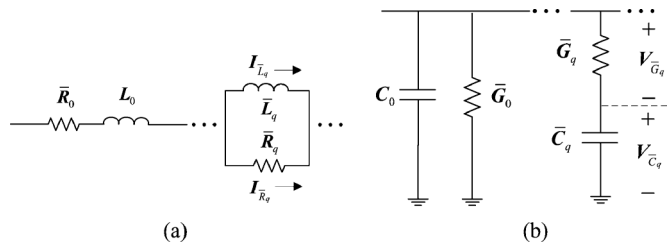

Fig. 2. Generalized equivalent circuits. (a) Representation of series impedance. (b) Representation of parallel admittance.

From Fig. 2, it is straightforward to obtain

$$\bar{\boldsymbol{R}}_q \boldsymbol{I}_{\bar{R}_q} = s\bar{\boldsymbol{L}}_q \boldsymbol{I}_{\bar{L}_q} \tag{7a}$$

$$\bar{\boldsymbol{G}}_q \boldsymbol{V}_{\bar{G}_q} = s\bar{\boldsymbol{C}}_q \boldsymbol{V}_{\bar{C}_q}. \tag{7b}$$

Combining (6a) and (6b) and (7a) and (7b), we have the relationships

$$\bar{R}_q^{j,k} I_{\bar{R}_q}^k = s\bar{L}_q^{j,k} I_{\bar{L}_q}^k \tag{8a}$$

$$\bar{G}_q^{j,k} V_{\bar{G}_q}^k = s\bar{C}_q^{j,k} V_{\bar{C}_q}^k \tag{8b}$$

where $j, k = 1, \ldots, N$. Despite their simplicity, these relationships are important for the derivation of relaxation sources in the WR-TP algorithm presented in Section III. They imply that the coupling effects of off-diagonal elements in $\bar{\boldsymbol{R}}_q$ and $\bar{\boldsymbol{L}}_q$ are essentially equivalent. Analogously, the coupling effects of the off-diagonal elements in $\bar{\boldsymbol{G}}_q$ and $\bar{\boldsymbol{C}}_q$ are also equivalent.

III. Implementation of Waveform Relaxation With Transverse Partitioning

A. Formulation of WR-TP for EMI Simulation

In the implementation of the WR-TP technique, the expressions of coupled transmission lines (2a) and (2b) should be written in the form of individual lines with relaxation sources. The resulting equations in a matrix form is given by

$$\frac{d\boldsymbol{\Phi}^{(r+1)}(z,s)}{dz} + \boldsymbol{D}(s)\boldsymbol{\Phi}^{(r+1)}(z,s) + \boldsymbol{P}(s)\boldsymbol{\Phi}^{(r)}(z,s) = \boldsymbol{K}(z,s) \tag{9a}$$

where

$$\boldsymbol{\Phi}^{(r+1)}(z,s) = \begin{bmatrix} \boldsymbol{V}^{(r+1)}(z,s) \\ \boldsymbol{I}^{(r+1)}(z,s) \end{bmatrix} \tag{9b}$$

$$\boldsymbol{D}(s) = \begin{bmatrix} \boldsymbol{0} & \mathrm{diag}(\boldsymbol{Z}(s)) \\ \mathrm{diag}(\boldsymbol{Y}(s)) & \boldsymbol{0} \end{bmatrix} \tag{9c}$$

$$\boldsymbol{P}(s) = \begin{bmatrix} \boldsymbol{0} & \mathrm{nondiag}(\boldsymbol{Z}(s)) \\ \mathrm{nondiag}(\boldsymbol{Y}(s)) & \boldsymbol{0} \end{bmatrix} \tag{9d}$$

$$\boldsymbol{K}(z,s) = \begin{bmatrix} \boldsymbol{F}(z,s) \\ \boldsymbol{0} \end{bmatrix}. \tag{9e}$$

Here, the functions diag and nondiag are used to obtain the diagonal and nondiagonal entries of a matrix, respectively.

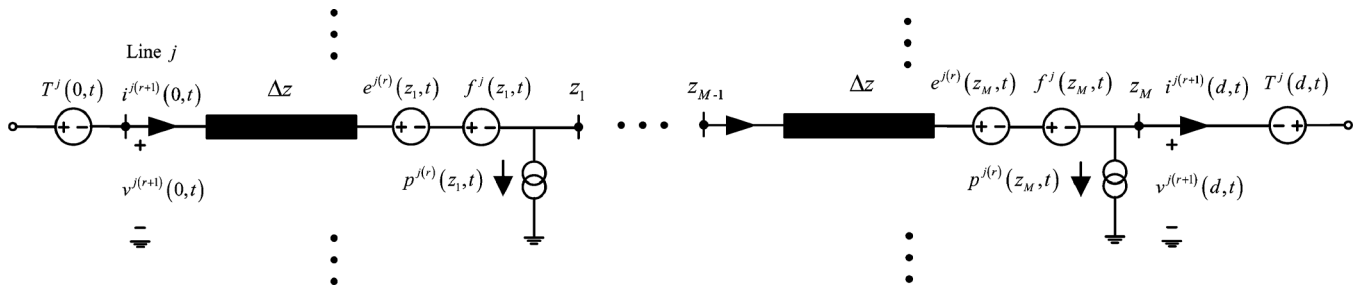

Fig. 3. Equivalent circuits representation for (10).

These equations can be solved as [17]

$$\begin{aligned}\boldsymbol{\Phi}^{(r+1)}(d) &= e^{-\boldsymbol{D}d}\boldsymbol{\Phi}^{(r+1)}(0) \\ &\quad + \int_0^d e^{-\boldsymbol{D}(d-\varsigma)}\left[\boldsymbol{K}(\varsigma) - \boldsymbol{P}\boldsymbol{\Phi}^{(r)}(\varsigma)\right]d\varsigma \\ &\cong e^{-\boldsymbol{D}d}\boldsymbol{\Phi}^{(r+1)}(0) \\ &\quad + \sum_{m=1}^{M} e^{-\boldsymbol{D}(d-z_m)}\left[\boldsymbol{K}(z_m) - \boldsymbol{P}\boldsymbol{\Phi}^{(r)}(z_m)\right]\Delta z\end{aligned} \tag{10}$$

where d is the total length of transmission lines and M is the number of discretization points. As indicated in [17], (10) can be realized using equivalent circuits in either the time or frequency domains. To integrate the model with SPICE-like circuit simulators [24] conveniently, the time-domain equivalent circuits are depicted in Fig. 3.

Notice that the scattered voltage in (10) should be transformed to the total voltage using (3a) and (3b) when connected with terminal loads in the circuit simulation. Therefore, additional voltage sources are placed at two terminals of each line, as shown in Fig. 3. They are given by

$$T^j(0,t) = -\int_{\rho^j(x,y)} E_t^j(\rho,0,t)d\rho \tag{11a}$$

$$T^j(d,t) = -\int_{\rho^j(x,y)} E_t^j(\rho,d,t)d\rho. \tag{11b}$$

Referring to Fig. 2, the equivalent circuit for one segment of the jth line in Fig. 3 can be realized in Fig. 4. The calculation of the relaxation voltage source $e^{j(r)}$ and current source $p^{j(r)}$ is described as follows.

As pointed out in Section II that $\bar{\boldsymbol{R}}_q$ and $\bar{\boldsymbol{L}}_q$ are in parallel and the coupling effects of off-diagonal elements in $\bar{\boldsymbol{R}}_q$ and $\bar{\boldsymbol{L}}_q$ are equivalent [see (8a)], we only need to consider one of them in $e^{j(r)}$ (e.g., in the derivation of this paper we choose the coupling of off-diagonal elements in $\bar{\boldsymbol{R}}_q$). The calculation of $p^{j(r)}$ can be done in a similar way. In addition, making use of the following relationships:

$$\bar{R}_q^{j,k} i_{\bar{R}_q}^k = \frac{\bar{R}_q^{j,k}}{\bar{R}_q^{k,k}} v_{\bar{R}_q}^k \tag{12a}$$

$$\bar{G}_q^{j,k} v_{\bar{G}_q}^k = \frac{\bar{G}_q^{j,k}}{\bar{G}_q^{k,k}} i_{\bar{G}_q}^k \tag{12b}$$

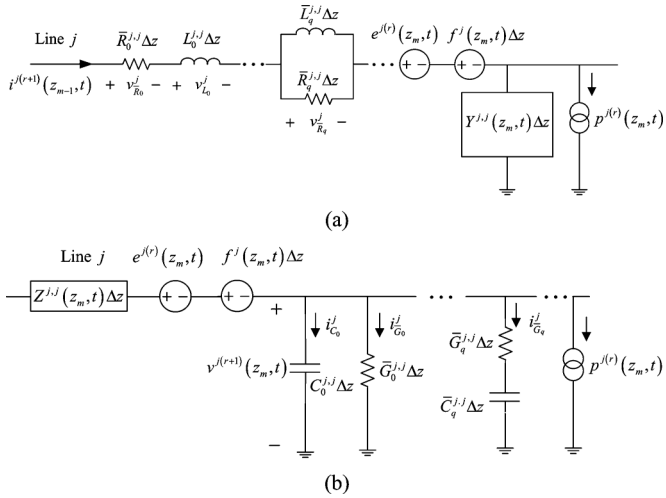

Fig. 4. Equivalent circuit for one segment of a single line.

the relaxation voltage and current sources in Fig. 4 can be written as

$$\begin{aligned}&e^{j(r)}(z_m,t) \\ &\quad = \sum_{k=1,k\neq j}^{N}\left[\frac{\bar{R}_0^{j,k}}{\bar{R}_0^{k,k}} v_{\bar{R}_0}^{k(r)} + \frac{L_0^{j,k}}{L_0^{k,k}} v_{L_0}^{k(r)} + \sum_{q=1}^{Q_1}\frac{\bar{R}_q^{j,k}}{\bar{R}_q^{k,k}} v_{\bar{R}_q}^{k(r)}\right]\end{aligned} \tag{13a}$$

$$\begin{aligned}&p^{j(r)}(z_m,t) \\ &\quad = \sum_{k=1,k\neq j}^{N}\left[\frac{\bar{G}_0^{j,k}}{\bar{G}_0^{k,k}} i_{\bar{G}_0}^{k(r)} + \frac{C_0^{j,k}}{C_0^{k,k}} i_{C_0}^{k(r)} + \sum_{q=1}^{Q_2}\frac{\bar{G}_q^{j,k}}{\bar{G}_q^{k,k}} i_{\bar{G}_q}^{k(r)}\right].\end{aligned} \tag{13b}$$

Note that the expression of (13a) and (13b) is much more compact than that in [18] and the derivation process is simple and clear.

In this way, the N-coupled transmission lines are partitioned into N single lines with relaxation sources, and the iteration calculation is executed until the convergence is achieved. The computational cost increases almost linearly with N [14], [18], providing a significant speed up as compared to conventional methods. Note that the force source $f^j(z_m,t)$ remains unchanged during the iteration. The calculation of $f^j(z_m,t)$ will be investigated in Section IV.

B. Strongly Coupled Transmission Lines

As mentioned in the previous literature on WR-TP [14], [17]–[19], the coupled transmission lines are partitioned in the

transverse direction taking advantage of the relatively weak coupling between individual traces. If several traces are placed close together, strong coupling between them will exist. In this case, they should be grouped together within the same sub-circuit [17]. This idea can be implemented in a straightforward way by making some modifications to the relaxation sources derived earlier in this section.

For simplicity and without loss of generality, it is assumed that strong coupling exists between the lines j, v, and w. Again, we consider the modeling of the jth line for example. The equivalent circuits described in Figs. 3 and 4 are still available, except that the relaxation voltage and current sources are required to be modified. They can be divided into two parts, one is for strong coupling from lines v and w, and the other is for the relatively weak coupling from other lines. The former is the controlled source of the $(r+1)$th iteration, while the latter is that of the rth iteration that is known. They can be described by

$$e^j(z_m,t) = e_1^{j(r+1)}(z_m,t) + e_2^{j(r)}(z_m,t) \tag{14a}$$

$$p^j(z_m,t) = p_1^{j(r+1)}(z_m,t) + p_2^{j(r)}(z_m,t) \tag{14b}$$

where

$$e_1^{j(r+1)}(z_m,t) = \sum_{k=v,w}\left[\frac{\bar{R}_0^{j,k}}{\bar{R}_0^{k,k}} v_{\bar{R}_0}^{k(r+1)} + \frac{L_0^{j,k}}{L_0^{k,k}} v_{L_0}^{k(r+1)} + \sum_{q=1}^{Q_1} \frac{\bar{R}_q^{j,k}}{\bar{R}_q^{k,k}} v_{\bar{R}_q}^{k(r+1)}\right] \tag{14c}$$

$$p_1^{j(r+1)}(z_m,t) = \sum_{k=v,w}\left[\frac{\bar{G}_0^{j,k}}{\bar{G}_0^{k,k}} i_{\bar{G}_0}^{k(r+1)} + \frac{C_0^{j,k}}{C_0^{k,k}} i_{C_0}^{k(r+1)} + \sum_{q=1}^{Q_2} \frac{\bar{G}_q^{j,k}}{\bar{G}_q^{k,k}} i_{\bar{G}_q}^{k(r+1)}\right] \tag{14d}$$

$$e_2^{j(r)}(z_m,t) = \sum_{k=1,k\neq j,v,w}^{N}\left[\frac{\bar{R}_0^{j,k}}{\bar{R}_0^{k,k}} v_{\bar{R}_0}^{k(r)} + \frac{L_0^{j,k}}{L_0^{k,k}} v_{L_0}^{k(r)} + \sum_{q=1}^{Q_1} \frac{\bar{R}_q^{j,k}}{\bar{R}_q^{k,k}} v_{\bar{R}_q}^{k(r)}\right] \tag{14e}$$

$$p_2^{j(r)}(z_m,t) = \sum_{k=1,k\neq j,v,w}^{N}\left[\frac{\bar{G}_0^{j,k}}{\bar{G}_0^{k,k}} i_{\bar{G}_0}^{k(r)} + \frac{C_0^{j,k}}{C_0^{k,k}} i_{C_0}^{k(r)} + \sum_{q=1}^{Q_2} \frac{\bar{G}_q^{j,k}}{\bar{G}_q^{k,k}} i_{\bar{G}_q}^{k(r)}\right]. \tag{14f}$$

The similar treatment can made for lines v and w, while other lines remain the expressions of (13a) and (13b).

It is worth noting that the term of "strong coupling" mentioned above is actually a relative concept. Whether several lines are suggested to be grouped together in a sub-circuit is not determined by the absolute values of coupling coefficients, but their relative values comparing with other lines.

IV. Modeling and Simulation of Dispersive Media

In this paper, it is assumed that the coupled interconnects are placed on or embedded in a dispersive substrate. In order to obtain the distribution voltage sources in (2a) produced by the external field coupling, the corresponding field quantities are calculated with the full-wave electromagnetic simulation in the absence of the conductors [12]. For accurate modeling, it is important to consider frequency variations of the dielectric parameters, which are available as table data provided by the manufacturers or described by standard physics-based formulations like the Debye or Lorentz models [2]–[4]. In practice, the multiterm Debye function expansion is suitable for modeling the dielectric behavior of most PCB materials (e.g., FR-4 in [2]).

Over the past two decades, approaches based on the Yee FDTD algorithm have been widely studied and developed for modeling dispersive materials [25]. In general, these methods can be divided into three basic categories: recursive convolution methods [26], [27], z-transform methods [28] and auxiliary differential equation (ADE) methods [29]–[32]. Recently, an equivalent-circuit FDTD method [33] has been proposed for the modeling of dispersive materials. A complete circuital formulation of the conventional FDTD was represented in this method. In [4], the similar equivalent-circuit representation was also exploited in the development of a PEEC formulation for dispersive media. In this section, however, our purpose is to calculate the fields in a dispersive substrate, the formulations based on the Maxwell equations are therefore more suitable.

A. ECM of Debye Media

For a Debye medium having Q poles, the expression of permittivity is written as

$$\varepsilon(s) = \varepsilon_0\varepsilon_\infty + \sum_{q=1}^{Q}\frac{\varepsilon_0\Delta\varepsilon_q}{1+s\tau_q} \tag{15}$$

where ε_0 is the permittivity of free space, ε_∞ is the permittivity at "infinite" frequency, $\Delta\varepsilon_q = \varepsilon_{s,q} - \varepsilon_{\infty,q}$ is the variation in relative permittivity due to the qth pole, and τ_q is the qth relaxation time. Without loss of generality, the Maxwell curl equation concerning the y-directed electric field is given by

$$\frac{\partial H_x}{\partial z} - \frac{\partial H_z}{\partial x} = \left(\varepsilon_0\varepsilon_\infty s + \sum_{q=1}^{Q}\frac{\varepsilon_0\Delta\varepsilon_q s}{1+j\omega\tau_q}\right)E_y. \tag{16}$$

In contrast to the traditional methods with the introduction of the electric polarization vector to develop ADEs [29], [31], a convenient technique based on the ECM is utilized here (the equivalence between the ECM and ADE formulations is explained in the Appendix). Inspired by the equivalent-circuit model of frequency-dependent interconnects in Section II, (16) can be represented by an admittance-type ECM, as shown in Fig. 5, where $C_0 = \varepsilon_0\varepsilon_\infty$, $C_q = \varepsilon_0\Delta\varepsilon_q$, $G_q = C_q/\tau_q$, $V = E_y$, $V_q = E'_{y(q)}$, and $I = \partial H_x/\partial z - \partial H_z/\partial x$.

Based on Kirchhoff's laws, it is straightforward to obtain the following differential equations in the time domain:

$$\frac{\partial H_x}{\partial z} - \frac{\partial H_z}{\partial x} = C_0\frac{dE_y}{dt} + \sum_{q=1}^{Q} C_q\frac{dE'_{y(q)}}{dt} \tag{17a}$$

and

$$-G_qE_y + G_qE'_{y(q)} + C_q\frac{dE'_{y(q)}}{dt} = 0 \tag{17b}$$

where $E'_{y(q)}$ is the auxiliary variable.

The FDTD algorithm is utilized to solve these coupled equations. The resulting update formula for E_y is given by

$$\begin{aligned} E_y^{n+1}&(i,j+1/2,k) \\ &= \frac{b_1}{a_1}E_y^n(i,j+1/2,k) \\ &\quad + \frac{1}{a_1}\sum_{q=1}^{Q} d_q E'^n_{y(q)}(i,j+1/2,k) \\ &\quad + \frac{1}{a_1\Delta z}\Big[H_x^{n+1/2}(i,j+1/2,k+1/2) \\ &\qquad\qquad - H_x^{n+1/2}(i,j+1/2,k-1/2)\Big] \\ &\quad - \frac{1}{a_1\Delta x}\Big[H_z^{n+1/2}(i+1/2,j+1/2,k) \\ &\qquad\qquad - H_z^{n+1/2}(i-1/2,j+1/2,k)\Big] \end{aligned} \tag{18a}$$

and the corresponding update equation for the auxiliary variable $E'_{y(q)}$ is written by

$$\begin{aligned} E'^{n+1}_{y(q)}&(i,j+1/2,k) \\ &= e_q E'^n_{y(q)}(i,j+1/2,k) \\ &\quad + f_q\left[E_y^{n+1}(i,j+1/2,k) + E_y^n(i,j+1/2,k)\right] \end{aligned} \tag{18b}$$

where

$$a_1 = \frac{C_0}{\Delta t} + \sum_{q=1}^{Q}\frac{C_q f_q}{\Delta t} \tag{18c}$$

$$b_1 = \frac{C_0}{\Delta t} - \sum_{q=1}^{Q}\frac{C_q f_q}{\Delta t} \tag{18d}$$

$$d_q = \frac{C_q}{\Delta t}(1-e_q) \tag{18e}$$

$$e_q = \frac{2C_q - G_q\Delta t}{2C_q + G_q\Delta t} \tag{18f}$$

$$f_q = \frac{G_q\Delta t}{2C_q + G_q\Delta t}. \tag{18g}$$

The similar update equations can be derived for E_x and E_z components. On the other side, the update equations for $\boldsymbol{H}$ are the same to the standard FDTD schemes, e.g.,

$$\begin{aligned} H_z^{n+1/2}&(i+1/2,j+1/2,k) \\ &= H_z^{n-1/2}(i+1/2,j+1/2,k) \\ &\quad + \frac{\Delta t}{\mu\Delta y}\left[E_x^n(i+1/2,j+1,k) - E_y^n(i+1/2,j,k)\right] \\ &\quad - \frac{\Delta t}{\mu\Delta x}\left[E_y^n(i+1,j+1/2,k) - E_y^n(i,j+1/2,k)\right]. \end{aligned} \tag{19}$$

Obtaining the electric field values from the full-wave simulation, the distributed force sources in (2a), as well as those in (3a), can be determined straightforwardly.

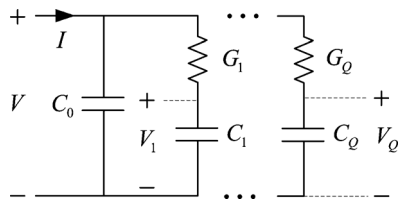

Fig. 5. Equivalent-circuit representation of multiterm Debye medium.

The accuracy of the algorithm can be evaluated by the numerical dispersion errors. Following the procedure in [34], the numerical permittivity can be derived as given by

$$\hat{\varepsilon} = C_0 + \sum_{q=1}^{Q}\frac{\Lambda C_q G_q}{\Lambda G_q + j\Omega C_q} \tag{20a}$$

where

$$\Omega = \frac{2}{\Delta t}\sin\left(\frac{\omega\Delta t}{2}\right) \tag{20b}$$

$$\Lambda = \cos\left(\frac{\omega\Delta t}{2}\right). \tag{20c}$$

Combining the expressions of lumped elements in Fig. 5, the numerical permittivity can be rewritten as

$$\hat{\varepsilon} = \varepsilon_0\varepsilon_\infty + \sum_{q=1}^{Q}\varepsilon_0\Delta\varepsilon_q\left(\frac{\Lambda}{\Lambda + j\Omega\tau_q}\right) \tag{21}$$

which is the same to the result of an ADE-based algorithm denoted as "D-DIM2" in [35]. Note that as Δt becomes infinitesimal, (21) will reduce to the exact expression of (15). The rate of convergence is second order.

Therefore, we can conclude that the numerical dispersion errors as well as stability of the ECM approach are the same as those of the ADE-based counterpart. Thus, they are not repeated here. The reader may refer to many excellent papers for detailed information [34]–[37].

B. ECM of Lorentz Media

As an extension, this ECM technique is readily exploited for modeling the Lorentz media as follows. For a Lorentz medium with Q poles, the expression of permittivity is given by

$$\varepsilon(s) = \varepsilon_0\varepsilon_\infty + \sum_{q=1}^{Q}\frac{\varepsilon_0\Delta\varepsilon_q\omega_q^2}{\omega_q^2 + 2\delta_q s + s^2} \tag{22}$$

where ω_q is the qth resonate frequency and δ_q is the qth damping coefficient. The corresponding ECM is shown in Fig. 6, where $C_0 = \varepsilon_0\varepsilon_\infty$, $C_q = \varepsilon_0\Delta\varepsilon_q$, $L_q = 1/\omega_q^2 C_q$, $R_q = 2\delta_q L_q$, $V = E_y$, $V_q = E'_{y(q)}$, $I_q = E''_{y(q)}$, and $I = \partial H_x/\partial z - \partial H_z/\partial x$.

Likewise, a set of differential equations derived from Kirchhoff's laws are given by

$$\frac{\partial H_x}{\partial z} - \frac{\partial H_z}{\partial x} = C_0\frac{dE_y}{dt} + \sum_{q=1}^{Q}E''_{y(q)} \tag{23a}$$

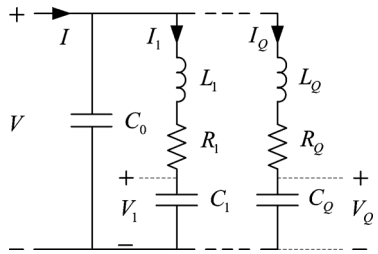

Fig. 6. Equivalent-circuit representation of multiterm Lorentz medium.

$$E'_y + R_q E''_{y(q)} + L_q \frac{dE''_{y(q)}}{dt} - E_y = 0 \tag{23b}$$

$$C_p \frac{dE'_{y(q)}}{dt} - E''_{y(q)} = 0 \tag{23c}$$

where $E'_{y(q)}$ and $E''_{y(q)}$ are both auxiliary variables. Similar to the case of the Debye medium, the FDTD algorithm is employed to solve these coupled equations. Due to space limitations, it is not presented here.

V. Numerical Results

In this section, four case studies are presented. The impact of dispersive dielectrics on the transient response of interconnects is illustrated in the first example. The capability of proposed method for the simulation of strongly coupled interconnects with nonlinear terminations is demonstrated in the second example. Incident field coupling to PCB traces with realistic features such as bends and vias are analyzed in the third example. The EMI simulation of the PCB placed in a metallic rectangular enclosure with multiple slots is given in the last example. For simplicity, a two-term Debye formulation is used to characterize the dispersive dielectric with $\varepsilon_\infty = 4.25$, $\Delta\varepsilon_1 = 0.15$, $\Delta\varepsilon_2 = 0.15$, $\tau_1 = 0.159$ ns, and $\tau_2 = 0.0159$ ns in all examples, and the p.u.l. frequency-dependent parameters of coupled interconnects are extracted using an electromagnetic simulator [38]. All the examples are executed using a PC with Pentium Dual Core CPU (2.27 GHz).

A. Microstrip Lines With Plane-Wave Excitation

In this example, the proposed method is compared with two existing techniques. One is the conventional technique where the medium surrounding the interconnects is treated as homogenous air in the calculation of incident field. It is referred to as the "conventional model" for convenience. The other is the physical optics approach, which is based on the assumption that the size of a layered medium is infinitely large. It is referred to hereafter as "PO" for short.

The test structure is the coupled microstrip lines on a dispersive substrate, and is exposed to an incident plane wave. The plane wave is a Gaussian pulse $E(t) = E_0 \exp\{-[(t-t_0)/\tau]^2\}$ with $E_0 = 1$ kV/m, $\tau = 166.78$ ps, and $t_0 = 0.7$ ns. The angles of incidence and polarization with respect to a spherical coordinate system are illustrated in Fig. 7, which are chosen to be $\theta = 30°$, $\phi = -90°$, and $\theta_E = 90°$ in this example. The horizontal dimensions of the substrate is 30 cm $\times$ 10 cm. The cross-sectional geometry of the interconnects and corresponding schematic circuit are depicted in Figs. 8 and 9, respectively.

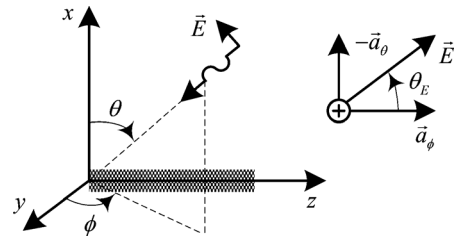

Fig. 7. Illustration of the definition of incident field as a uniform plane wave.

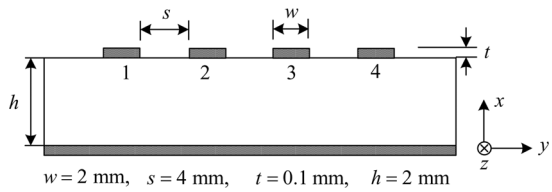

Fig. 8. Cross-sectional view of the microstrip structure.

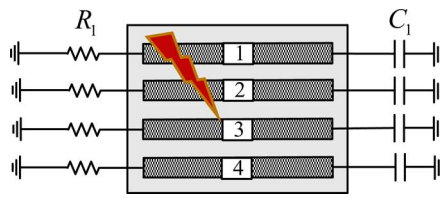

Fig. 9. Schematic circuit of the coupled lines.

Each line is terminated with a 50-Ω resistor and a 1-pF capacitor at the near and far ends. The length of the line is 20 cm. In contrast to the conventional model, the proposed method employs full-wave simulation to accurately model the field in a dispersive substrate. The convolutional perfect matched layer (CPML) [25] absorbing boundary is employed to truncate the computational domain. After that, transmission-line equations with distributed sources are solved using the WR-TP technique. The simulation results of transient voltages at the near and far ends of line #1 are depicted in Figs. 10 and 11. To validate the accuracy of the proposed method, the reference values are provided by a 3-D electromagnetic simulator Computer Simulation Technology (CST) [39]. As shown in the figures, the simulation results of the proposed method are in very good agreement with those of CST. In contrast, poor results from the conventional model are observed, especially at the far end of the line. Note that a similar phenomenon was also observed in [12], where the incident field coupling to interconnects with nondispersive dielectrics was studied, and the explanations were provided as well.

We then investigate the accuracy of PO method in simulating the same structure. The implementation of the PO method [11] also involves two stages, one is the electromagnetic calculation based on the PO principle and the other is the circuit simulation. Since the PO approach is based on the assumption that a layered medium extends to infinity in the lateral dimensions, its accuracy will suffer when the finite substrate is simulated, especially with large incidence angles. To illustrate this phenomenon, the transient responses at two ends of the interconnects with the incidence angle $\theta = 75°$ are depicted in Figs. 12 and 13. The divergence of the PO results is obvious. In contrast, the results of the proposed method agree quite well with the CST references.

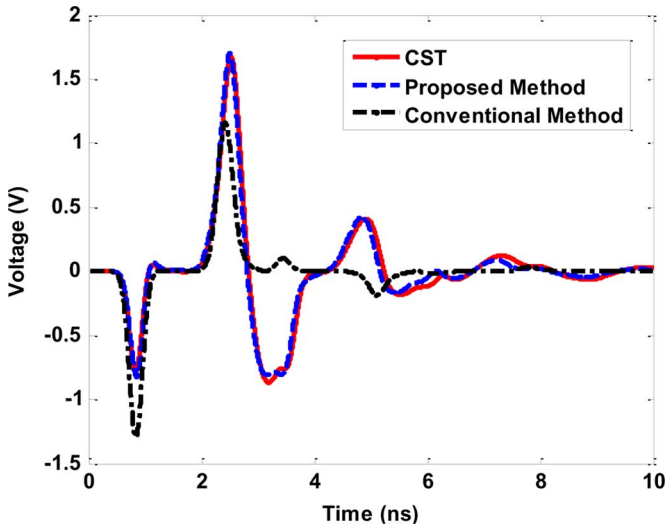

Fig. 10. Transient response of voltage at the near end (line #1) when $\theta = 30°$.

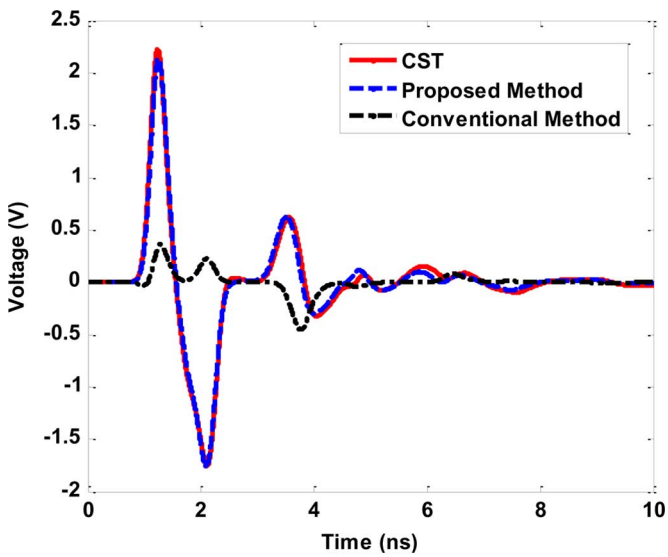

Fig. 11. Transient response of voltage at the far end (line #1) when $\theta = 30°$.

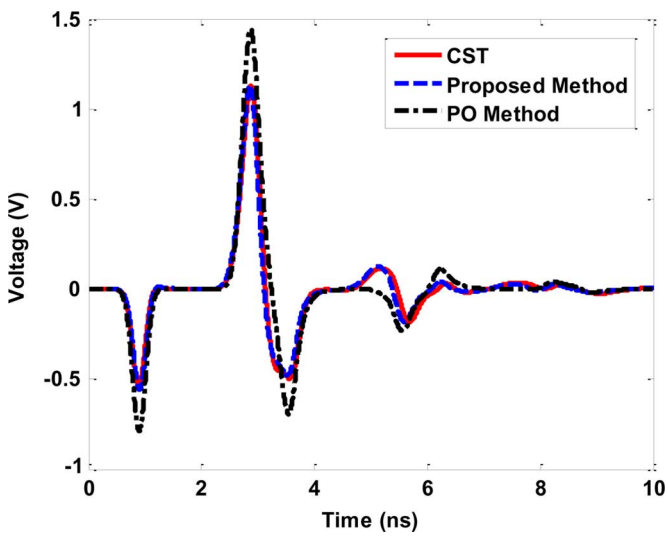

Fig. 12. Transient response of voltage at the near end (line #1) when $\theta = 75°$.

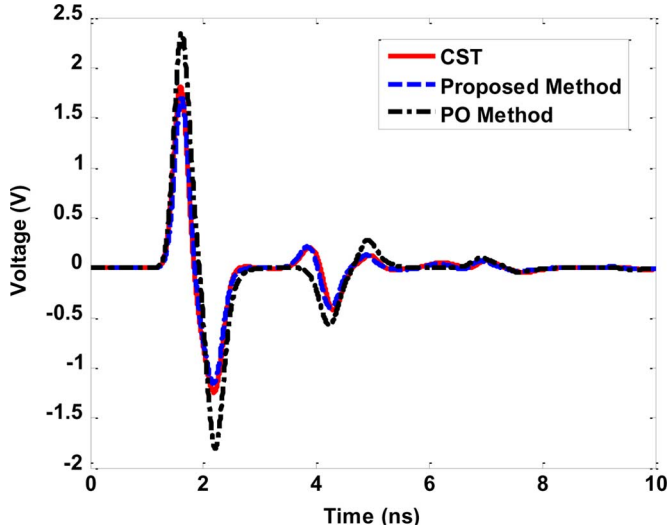

Fig. 13. Transient response of voltage at the far end (line #1) when $\theta = 75°$.

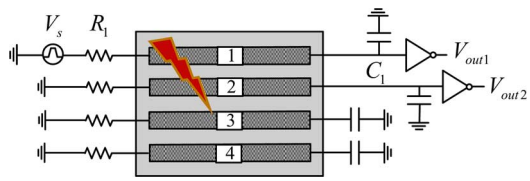

Fig. 14. Schematic circuit of coupled lines with nonlinear terminations.

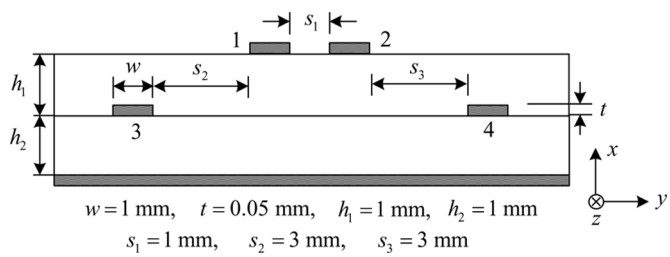

Fig. 15. Cross-sectional view of the interconnects.

B. Incident Filed Coupling to Nonlinear Circuit

The objective of this example is to predict the effect of the incident field on the nonlinear circuit operation. The schematic circuit is depicted in Fig. 14, where two COMS converters are terminated at the far end of the interconnection system. The length of each line is 5 cm. The EMI excitation is a Gaussian pulse with $E_0 = 1.7$ kV/m, $\tau = 166.78$ ps, and $t_0 = 4.5$ ns. The angles of incidence and polarization are $\theta = 30°$, $\phi = -90°$, and $\theta_E = 90°$. The input voltage source of the circuit is a 5-V pulse with 0.5-ns rise/fall time and width of 2.5 ns. The values of resistors and capacitors are 50 Ω and 1 pF. A cross-sectional view of the physical structure is described in Fig. 15. It is observed that lines #1 and #2 are placed close to each other, and thus the electromagnetic coupling between them is much larger than other lines. According to the principle presented in Section III-B, they are suggested to be grouped together within the same subcircuit in WR-TP simulation to achieve fast convergence. The simulation results are described in Figs. 16 and 17, where both conditions with and without EMI

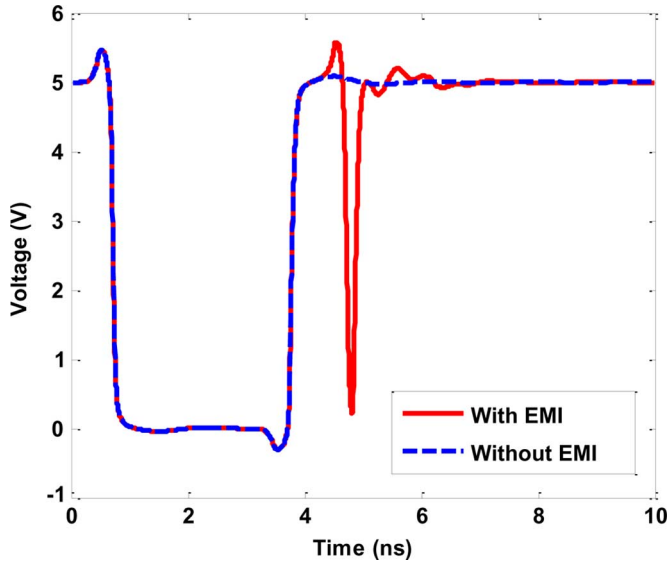

Fig. 16. Transient voltage at the output of inverter (line #1).

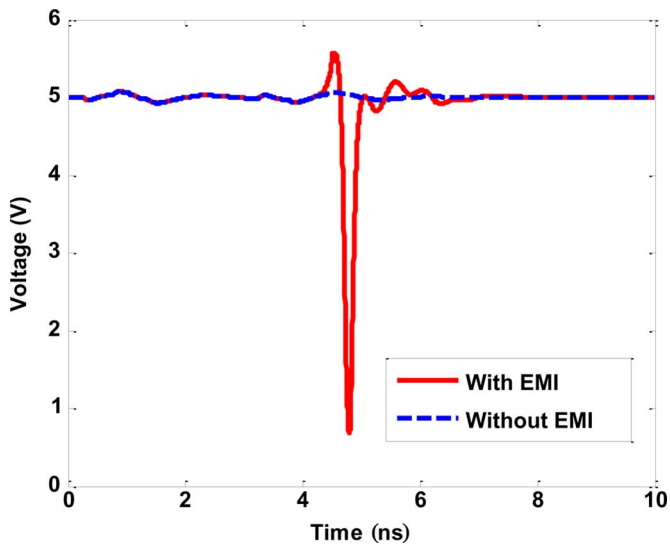

Fig. 17. Transient voltage at the output of inverter (line #2).

disturbances are given for comparison. The convergence of simulation is achieved after three iterations (with the maximum tolerance $\leq 10^{-3}$ V) using the proposed method. However, if lines #1 and #2 are separated and simulated in individual sub-circuits, five iterations are required to achieve the convergence within the same tolerance.

C. EMI Analysis of Traces With Bends and Vias

In this example, the PCB traces with realistic features such as bends and vias are investigated. The first structure is the embedded microstrip lines with two bends, and the second one consists of traces with different lengths connected by two vias. The schematic circuits are depicted in Fig. 18, where the loads are all 50-Ω resistors. The voltage source of line #2 in the second circuit is a 1-V pulse with 0.5-ns rise/fall time and width of 2 ns. The cross-sectional view at the position of dash line is described in Fig. 19. For both cases, the EMI excitation is assumed to be the same Gaussian pulse with $E_0 = 1$ kV/m, $\tau = 166.78$ ps, and $t_0 = 0.7$ ns. The angles of incidence and polarization are

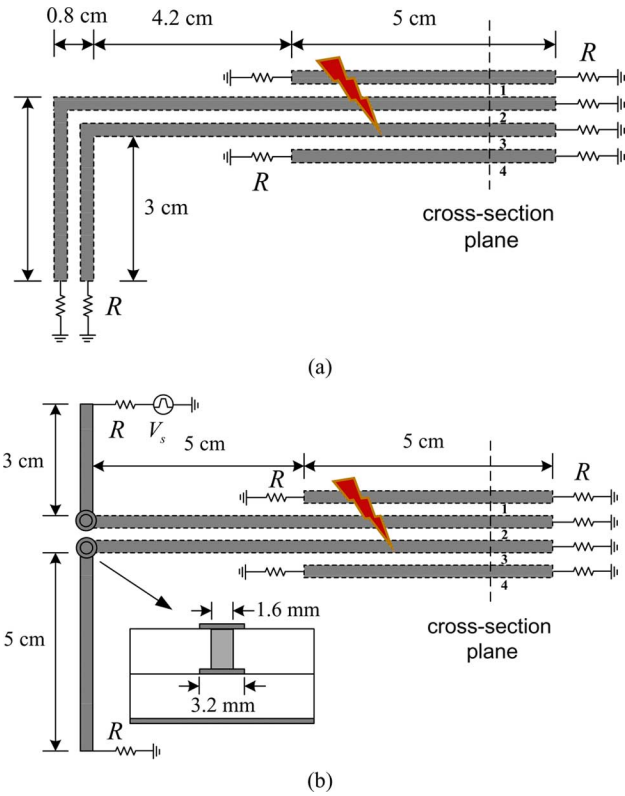

Fig. 18. Schematic circuits of PCB traces with bends and vias.

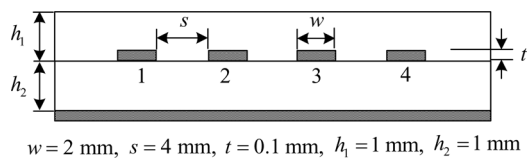

Fig. 19. Cross-sectional view of the embedded microstrip structure.

$\theta = 30°$, $\phi = -90°$, and $\theta_E = 90°$. Since the substrate and external incident field remain unchanged, full-wave electromagnetic calculation needs to be carried out only once to capture accurate field in a dispersive substrate. These field values will then be reused in the circuit simulation for both cases. It is one of the intrinsic advantages of the proposed method over the conventional full-wave solvers, where different circuit topologies are required to be simulated repeatedly using the full-wave algorithms. In the circuit simulation stage, the modeling of bends is referred to [40], while that of the vias is from [41] and [42]. For the first structure, the transient voltage at the far end of line #3 is described in Fig. 20. With the excitation of a voltage source, as well as the external-field coupling, the transient response at the far end of line #2 is depicted in Fig. 21 for the second topology. It is observed that the simulation results of the proposed method are in good agreement with the CST references in both cases.

D. EMI Analysis of PCB in Metallic Enclosure

Furthermore, a typical EMI analysis of the PCB placed in a metallic rectangular enclosure with multiple slots is provided in this example. The whole structure is described in Fig. 22, where the slot width is 2 mm. The incident wave is a Gaussian pulse

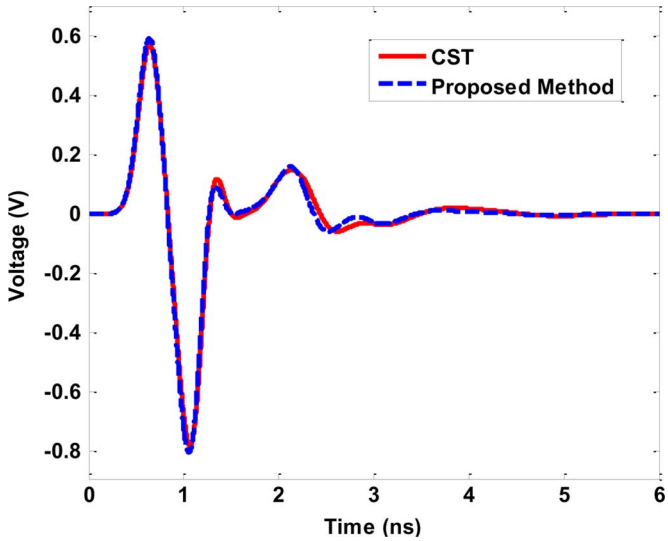

Fig. 20. Transient voltage at the far end (line #3).

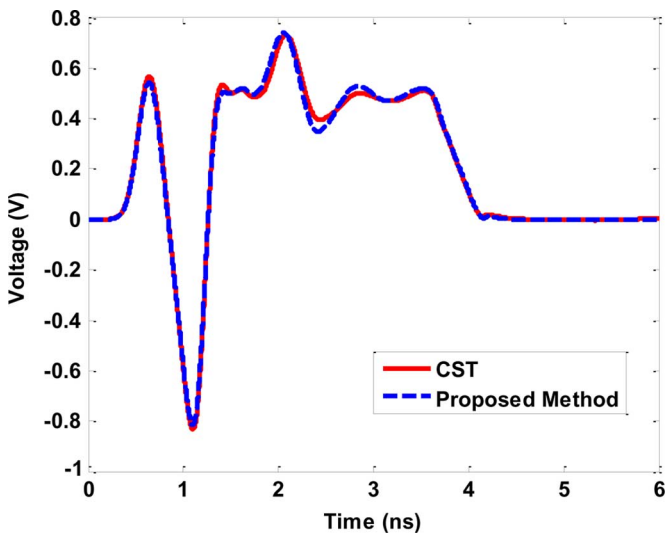

Fig. 21. Transient voltage at the far end (line #2).

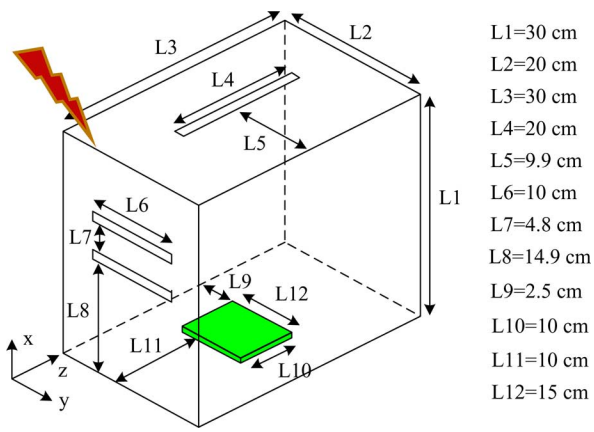

Fig. 22. Geometry of a rectangular metallic enclosure.

with $E_0 = 1$ kV/m, $\tau = 166.78$ ps, and $t_0 = 0.3$ ns. It propagates in the direction of $\theta = 45°$ and $\phi = -90°$ with a polarization angle $\theta_E = 90°$. The cross-sectional geometry of the PCB is depicted in Fig. 23. Like the previous example, two circuit topologies are studied, as shown in Fig. 24. The first structure

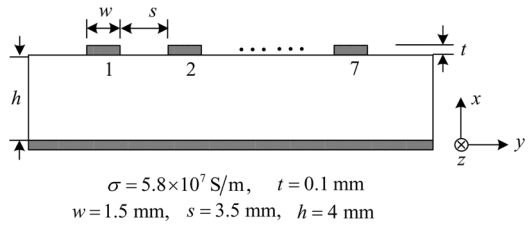

Fig. 23. Cross-sectional view of the PCB.

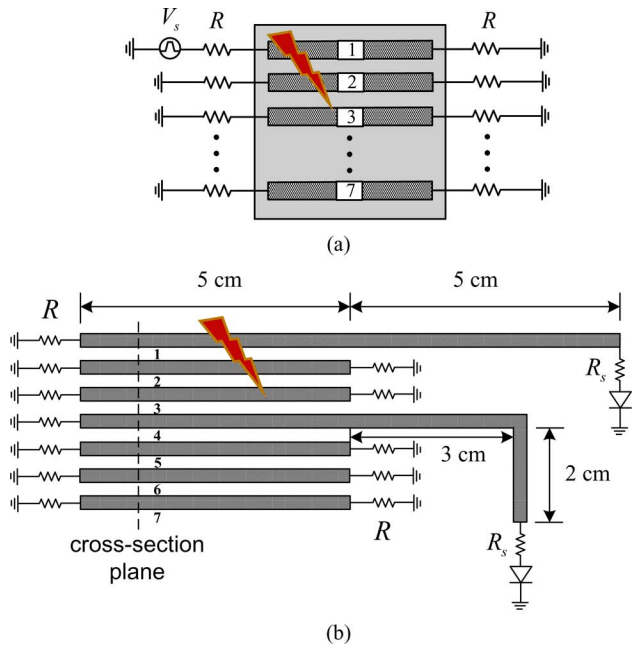

Fig. 24. Schematic circuits of PCB with different topologies.

consists of seven parallel traces with 10-cm length and terminated with 50-Ω resistors at the near and far ends. The input voltage source of the circuit is a 1-V pulse with a 0.5-ns rise/fall time and a width of 3 ns. The second topology is more complicated with different trace lengths, including a bend structure. At the far ends of lines #1 and #4, two diodes in series with 10-Ω resistors are terminated. The loads at other ends of the traces are all 50-Ω resistors. As mentioned in the previous example, for different circuit topologies we only need to perform full-wave calculation once. Note that in the full-wave simulation with FDTD algorithm, the thin slots on the metallic enclosure need special treatment. An improved formulation based on the conformal mapping technique [43] is exploited in this example to obtain an exact field distribution near the slot. As mentioned in Section IV, the metallic traces do not need to be considered when computing the excitation fields. Therefore, the computational resource of the proposed method is much less than that of the conventional full-wave algorithms where the traces are also meshed. To further improve the efficiency, the nonuniform grids [25] are utilized in the calculation of electromagnetic field in the cavity. The minimum and maximum mesh sizes are 2 and 5 mm, respectively. The simulation results for the two circuit topologies are shown in Figs. 25 and 26, respectively. For comparison, the results of the full-wave simulator CST are also depicted in the figures. It is observed that the results of two methods agree well with each other. For each case, the total simulation time

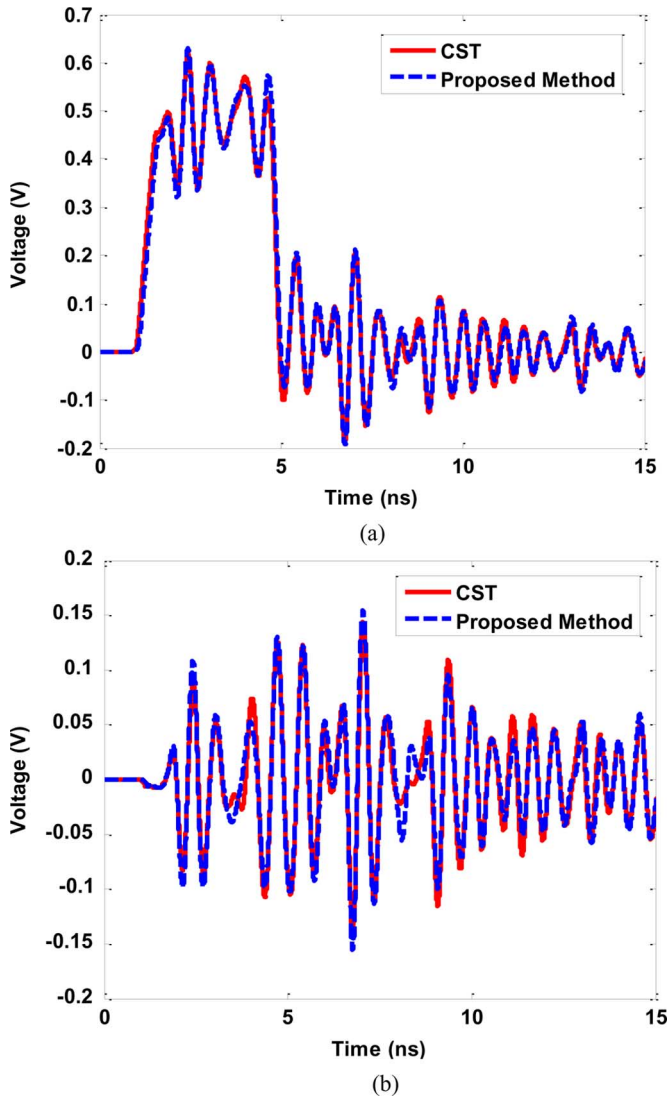

Fig. 25. Transient responses of the first circuit topology. (a) At the far end of line #1. (b) At the far end of line #4.

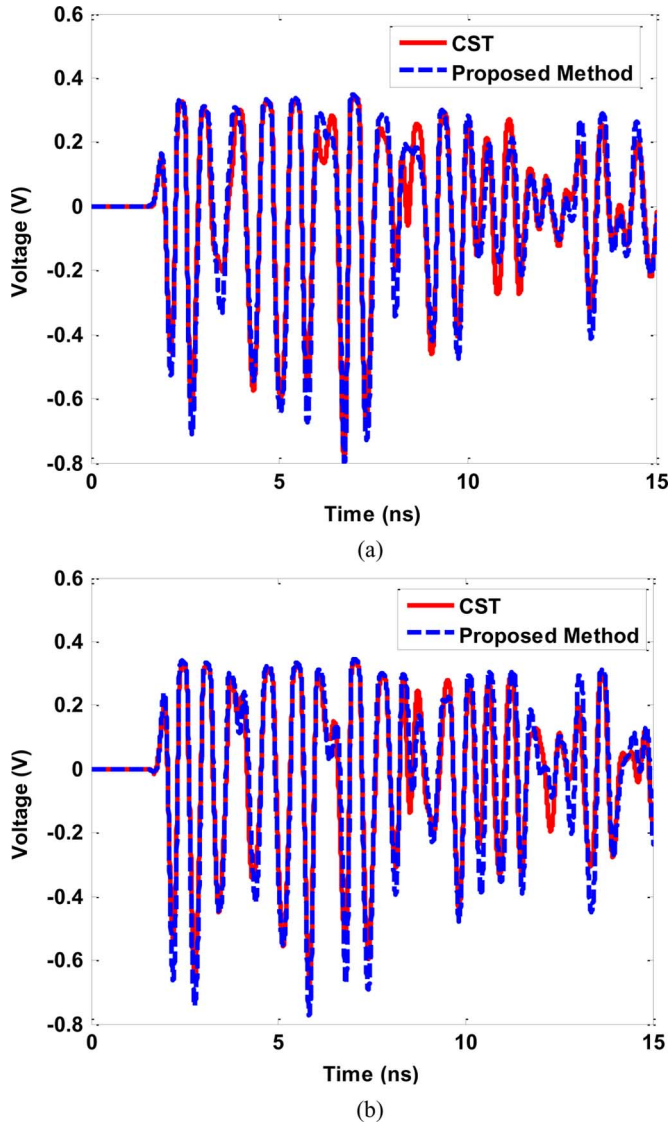

Fig. 26. Transient responses of the second circuit topology. (a) At the far end of line #1. (b) At the far end of line #4.

of the proposed method is around 4 min, while that of CST is more than 27 min. Considering the fact that the full-wave simulation needs to be done only once in the proposed method, further speedup can be achieved.

VI. Conclusion

A hybrid method has been proposed for the simulation of interconnects on a dispersive substrate with incident field coupling. Based on the differential equations derived from the ECM of dispersive media, the full-wave FDTD algorithm is utilized to capture accurate field surrounding the interconnects. The impact of the dispersive dielectric is accurately incorporated in the field coupling model of transmission lines. The WR-TP technique is employed for efficient simulation of interconnects with distributed sources. The coupling effects between the lines are represented by the equivalent relaxation sources. A simple and clear derivation of the relaxation sources is described in this paper and the compact results are provided. The accuracy, efficiency, and applicability of the proposed method have been demonstrated by several benchmark examples.

Appendix

The FDTD algorithm based on ADEs is a typical technique for modeling dispersive materials. The ADEs can be obtained either by the constitutive relation involving the electric flux density and the electric field intensity [32] or the dynamic evolution of the polarization parameters excited by the propagating electric field [29]–[31]. A comparison between the latter ADE approach (called the Kashiwa's method for convenience) and the ECM utilized in this paper is given as follows.

A. Debye Media

In [29], differential equations for the Debye medium were written in the following state equation form:

$$\nabla \times \boldsymbol{H} = \varepsilon_0 \varepsilon_\infty \frac{\partial \boldsymbol{E}}{\partial t} + \frac{1}{\tau}[\varepsilon_0(\varepsilon_s - \varepsilon_\infty)\boldsymbol{E} - \boldsymbol{P}] \quad \text{(A.1a)}$$

$$\frac{\partial \boldsymbol{P}}{\partial t} = \frac{1}{\tau}[\varepsilon_0(\varepsilon_s - \varepsilon_\infty)\boldsymbol{E} - \boldsymbol{P}] \quad \text{(A.1b)}$$

where $\boldsymbol{P}$ is the polarization vector.

These equations can be extended to the multiterm expression cases with ease [31], described as follows:

$$\nabla \times \boldsymbol{H} = \varepsilon_0 \varepsilon_\infty \frac{\partial \boldsymbol{E}}{\partial t} + \sum_{q=1}^{Q} \frac{1}{\tau_q} [\varepsilon_0 (\varepsilon_{s,q} - \varepsilon_{\infty,q}) \boldsymbol{E} - \boldsymbol{P}_q] \tag{A.2a}$$

$$\frac{\partial \boldsymbol{P}_q}{\partial t} = \frac{1}{\tau_q} [\varepsilon_0 (\varepsilon_{s,q} - \varepsilon_{\infty,q}) \boldsymbol{E} - \boldsymbol{P}_q]. \tag{A.2b}$$

By introducing the following relationship:

$$\boldsymbol{P}_q = \varepsilon_0 (\varepsilon_{s,q} - \varepsilon_{\infty,q}) \boldsymbol{E'}_{(q)} \tag{A.3}$$

we can obtain the differential equations (17a) and (17b) proposed in Section IV.

B. Lorentz Media

In [31], the curl equations coupled with the ADEs for the Qth -order Lorentz medium is described by

$$\nabla \times \boldsymbol{H} = \varepsilon_0 \varepsilon_\infty \frac{\partial \boldsymbol{E}}{\partial t} + \sum_{q=1}^{Q} \boldsymbol{J}_{p(q)} \tag{A.4a}$$

$$\frac{\partial \boldsymbol{J}_{p(q)}}{\partial t} = \varepsilon_0 (\varepsilon_{s,q} - \varepsilon_{\infty,q}) \omega_0^2 \boldsymbol{E} - \omega_0^2 \boldsymbol{P}_q - 2\delta \boldsymbol{J}_{p(q)} \tag{A.4b}$$

$$\frac{\partial \boldsymbol{P}_q}{\partial t} = \boldsymbol{J}_{p(q)} \tag{A.4c}$$

where $\boldsymbol{J}_{p(q)}$ is the polarization current density.

These equations can be proven to be identical to (23a)–(23c) by assuming

$$\boldsymbol{P}_q = \varepsilon_0 (\varepsilon_{s,q} - \varepsilon_{\infty,q}) \boldsymbol{E'}_{(q)} \tag{A.5a}$$

$$\boldsymbol{J}_{p(q)} = \boldsymbol{E''}_{(q)}. \tag{A.5b}$$

Consequently, from the comparison above, we obtain that differential equations based on the ECM are equivalent to those in the Kashiwa's method.

REFERENCES

[1] A. Deutsch *et al.*, "Frequency-dependent losses on high-performance interconnections," *IEEE Trans. Electromagn. Compat.*, vol. 43, no. 4, pp. 446–465, Nov. 2001.

[2] A. R. Djordjević, R. M. Biljić, V. D. Likar-Smiljanić, and T. K. Sarkar, "Wideband frequency-domain characterization of FR-4 and time-domain causality," *IEEE Trans. Electromagn. Compat.*, vol. 43, no. 4, pp. 662–667, Nov. 2001.

[3] K. M. C. Branch, J. Morsey, A. C. Cangellaris, and A. E. Ruehli, "Physically consistent transmission line models for high-speed interconnects in lossy dielectrics," *IEEE Trans. Adv. Packag.*, vol. 25, no. 2, pp. 129–135, May 2002.

[4] G. Antonini, A. E. Ruehli, and C. Yang, "PEEC modeling of dispersive and lossy dielectrics," *IEEE Trans. Adv. Packag.*, vol. 31, no. 4, pp. 768–782, Nov. 2008.

[5] F. M. Tesche, M. V. Ianoz, and T. Karlsson, *EMC Analysis Methods and Computational Models*. New York: Wiley, 1997.

[6] C. R. Paul, *Analysis of Multiconductor Transmission Lines*, 2nd ed. New York: Wiley, 2008.

[7] C. D. Taylor, R. S. Satterwhite, and C. W. Harrison, "The response of a terminated two-wire transmission line excited by a nonuniform electro-magnetic field," *IEEE Trans. Antennas Propag.*, vol. AP-13, no. 6, pp. 987–989, Nov. 1965.

[8] A. K. Agrawal, H. J. Prince, and S. H. Gurbaxani, "Transient response of multiconductor transmission lines excited by a nonuniform electromagnetic field," *IEEE Trans. Electromagn. Compat.*, vol. EMC-22, no. 2, pp. 119–129, May 1980.

[9] F. Rachidi, "Formulation of field to field-to-transmission line coupling equations in terms of magnetic excitation," *IEEE Trans. Electromagn. Compat.*, vol. 35, no. 3, pp. 404–407, Aug. 1993.

[10] I. Maio and F. Canavero, "Analysis of crosstalk and field coupling to lossy MTLs in a SPICE environment," *IEEE Trans. Electromagn. Compat.*, vol. 38, no. 3, pp. 221–229, Aug. 1996.

[11] I. Erdin, R. Khazaka, and M. Nakhla, "Simulation of high-speed interconnects in a multilayered medium in the presence of incident field," *IEEE Trans. Microw. Theory Techn.*, vol. 46, no. 12, pp. 2251–2257, Dec. 1998.

[12] T. Lapohos, J. L. Vetri, and J. Seregelyi, "External field coupling to MTL networks with nonlinear junctions: Numerical modeling and experimental validation," *IEEE Trans. Electromagn. Compat.*, vol. 42, no. 1, pp. 16–29, Feb. 2000.

[13] G. S. Shinh, N. M. Nakhla, R. Achar, M. S. Nakhla, A. Dounavis, and I. Erdin, "Fast transient analysis of incident field coupling to multiconductor transmission lines," *IEEE Trans. Electromagn. Compat.*, vol. 48, no. 1, pp. 57–73, Feb. 2006.

[14] A. R. Sridhar, N. M. Nakhla, R. Achar, M. S. Nakhla, and A. E. Ruehli, "Fast EMI analysis via transverse partitioning and waveform relaxation," *IEEE Trans. Electromagn. Compat.*, vol. 51, no. 2, pp. 358–371, May 2009.

[15] G. Antonini, "A spectral formulation for the transient analysis of plane-wave coupling to multiconductor transmission lines," *IEEE Trans. Electronagn. Compat.*, vol. 51, no. 3, pp. 792–804, Aug. 2009.

[16] A. Dounavis, R. Achar, and M. Nakhla, "Efficient passive circuit models for distributed networks with frequency-dependent parameters," *IEEE Trans. Adv. Packag.*, vol. 23, no. 3, pp. 382–392, Aug. 2000.

[17] N. M. Nakhla, A. E. Ruehli, M. S. Nakhla, and R. Achar, "Simulation of coupled interconnects using waveform relaxation and transverse partitioning," *IEEE Trans. Adv. Packag.*, vol. 29, no. 1, pp. 78–87, Feb. 2006.

[18] N. Nakhla, A. E. Ruehli, M. S. Nakhla, R. Achar, and C. Chen, "Waveform relaxation techniques for simulation of coupled interconnects with frequency-dependent parameters," *IEEE Trans. Adv. Packag.*, vol. 30, no. 2, pp. 257–269, May 2007.

[19] D. Paul, N. M. Nakhla, R. Achar, and M. S. Nakhla, "Parallel simulation of massively coupled interconnect networks," *IEEE Trans. Adv. Packag.*, vol. 33, no. 1, pp. 115–127, Feb. 2010.

[20] B. Gustavsen and A. Semlyen, "Rational approximation of frequency domain responses by vector fitting," *IEEE Trans. Power Del.*, vol. 14, no. 3, pp. 1052–1061, Jul. 1999.

[21] D. Saraswat, R. Achar, and M. Nakhla, "A fast algorithm and practical considerations for passive macromodeling of measured/simulated data," *IEEE Trans. Adv. Packag.*, vol. 27, no. 1, pp. 57–70, Feb. 2004.

[22] K. M. Coperich, J. Morsey, V. I. Okhmatovski, A. C. Cangellaris, and A. E. Ruehli, "Systematic development of transmission line models for interconnects with frequency-dependent losses," *IEEE Trans. Microw. Theory Techn.*, vol. 49, no. 10, pp. 1677–1685, Oct. 2001.

[23] M. Tang and J. F. Mao, "A precise time-step integration method for transient analysis of lossy nonuniform transmission lines," *IEEE Trans. Electromagn. Compat.*, vol. 50, no. 1, pp. 166–174, Feb. 2008.

[24] *"Hspice User's Manual"* Synopsys Inc., Mountain View, CA, 2007. [Online]. Available: http://www.synopsys.com

[25] A. Taflove and S. C. Hagness, *Computational Electrodynamics: The Finite-Difference Time-Domain Method*, 3rd ed. Norwood, MA: Artech House, 2005.

[26] R. Luebbers, F. P. Hunsberger, K. S. Kunz, R. B. Standler, and M. Schneider, "A frequency-dependent finite-difference time-domain formulation for dispersive materials," *IEEE Trans. Electromagn. Compat.*, vol. 32, no. 3, pp. 222–227, Aug. 1990.

[27] D. F. Kelley and R. J. Luebbers, "Piecewise linear recursive convolution for dispersive media using FDTD," *IEEE Trans. Antennas Propag.*, vol. 44, no. 6, pp. 792–797, Jun. 1996.

[28] D. M. Sullivan, "Z-transform theory and the FDTD method," *IEEE Trans. Antennas Propag.*, vol. 44, no. 1, pp. 28–34, Jan. 1996.

[29] T. Kashiwa, N. Yoshida, and I. Fukai, "A treatment by the finite-difference time-domain method of the dispersive characteristics associated with orientation polarization," *IEICE Trans.*, vol. E73, no. 8, pp. 1326–1328, 1990.

[30] T. Kashiwa and I. Fukai, "A treatment by FDTD method of dispersive characteristics associated with electronic polarization," *Microw. Opt. Technol. Lett.*, vol. 3, pp. 203–205, 1990.

[31] J. L. Young, "Propagation in linear dispersive media: Finite difference time-domain methodologies," *IEEE Trans. Antennas Propag.*, vol. 43, no. 4, pp. 422–426, Apr. 1995.
[32] R. M. Joseph, S. C. Hagness, and A. Taflove, "Direct time integration of Maxwell's equations in linear dispersive media with absorption for scattering and propagation of femtosecond electromagnetic pulses," *Opt. Lett.*, vol. 16, no. 18, pp. 1412–1414, 1991.
[33] A. Rennings, J. Mosig, C. Caloz, D. Erni, and P. Waldow, "Equivalent circuit (EC) FDTD method for the modeling of surface plasmon based couplers," *J. Comput. Theoret. Nanosci.*, vol. 5, no. 4, pp. 690–703, Apr. 2008.
[34] J. L. Young, A. Kittichartphayak, Y. M. Kwok, and D. Sullivan, "On the dispersion errors related to $(FD)^2$ TD type schemes," *IEEE Trans. Microw. Theory Techn.*, vol. 43, no. 8, pp. 1902–1909, Aug. 1995.
[35] J. L. Young and R. O. Nelson, "A summary and systematic analysis of FDTD algorithms for linearly dispersive media," *IEEE Antennas Propag. Mag.*, vol. 43, no. 2, pp. 61–77, Feb. 2001.
[36] P. G. Petropoulos, "Stability and phase error analysis of FD-TD in dispersive dielectrics," *IEEE Trans. Antennas Propag.*, vol. 42, no. 1, pp. 62–69, Jan. 1994.
[37] L. Zhili and L. Thylen, "On the accuracy and stability of several widely used FDTD approaches for modeling Lorentz dielectrics," *IEEE Trans. Antennas Propag.*, vol. 57, no. 10, pp. 3378–3381, Oct. 2009.
[38] Q3D Extractor. ver. 8, Ansoft Corporation, Pittsburgh, PA, 2008. [Online]. Available: http://www.ansoft.com
[39] CST Studio Suite. Comput. Simulation Technol. (CST), Framingham, MA, 2009. [Online]. Available: www.cst.com
[40] K. C. Gupta, R. Garg, and I. J. Bahl, *Microstrip Lines and Slotlines*, 2nd ed. Norwood, MA: Artech House, 1996.
[41] I. Novak and J. R. Miller, *Frequency-Domain Characterization of Power Distribution Networks*. Norwood, MA: Artech House, 2007.
[42] M. Pajovic, "A closed-form equation for estimating capacitance of signal vias in arbitarily multilayered PCBs," *IEEE Trans. Electromagn. Compat.*, vol. 50, no. 4, pp. 966–973, Nov. 2008.
[43] C. T. Wu, Y. H. Pang, and R. B. Wu, "An improved formalism for FDTD analysis of thin-slot problems by conformal mapping technique," *IEEE Trans. Antennas Propag.*, vol. 51, no. 9, pp. 2530–2533, Sep. 2003.

Min Tang (M'09) received the B.S. degree in electronic engineering from Northwestern Polytechnical University, Xi'an, China, in 2001, the M.S. degree in electrical engineering from Xi'an Jiao Tong University, Xi'an, China, in 2004, and the Ph.D. degree in electronic engineering from Shanghai Jiao Tong University, Shanghai, China, in 2007.

He is currently a Lecturer with the Department of Electronic Engineering, Shanghai Jiao Tong University. His research interests include modeling and simulation of high-speed interconnects, computer-aided design (CAD) of very large scale integration (VLSI) circuits, and computational electromagnetics.

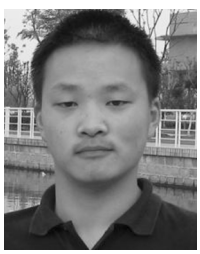

Jiaqing Lu received the B.S. degree in electronic engineering from Shanghai Jiao Tong University, Shanghai, China, in 2010, and is currently working toward the M.S. degree in electronic engineering at Shanghai Jiao Tong University.

His research interests include EMC and high-speed interconnects simulation.

Jun-Fa Mao (M'92–SM'98–F'11) was born in 1965. He received the B.S. degree in radiation physics from the University of Science and Technology of National Defense, Hefei, China, in 1985, the M.S. degree in experimental nuclear physics from the Shanghai Institute of Nuclear Research, Shanghai, China, in 1988, and the Ph.D. degree in electronic engineering from Shanghai Jiao Tong University, Shanghai, China, in 1992.

Since 1992, he has been a Faculty Member with Shanghai Jiao Tong University, where he is currently a Chair Professor and the Executive Dean of the School of Electronic, Information and Electrical Engineering. From 1994 to 1995, he was a Visiting Scholar with the Chinese University of Hong Kong, Kowloon, Hong Kong. From 1995 to 1996, he was a Postdoctoral Researcher with the University of California at Berkeley. is a Chief Scientist of The National Basic Research Program (973 Program) of China, a Project Leader of the National Science Foundation for Creative Research Groups of China, a Cheung Kong Scholar of the Ministry of Education, China, and an Associate Director of the Microwave Society of China Institute of Electronics. He has authored or coauthored over 190 journal papers (including 75 IEEE journal papers) and 120 international conference papers. His research interests include the interconnect and package problem of integrated circuits and systems and the analysis and design of microwave circuits.

Dr. Mao was the 2007–2009 chair of the IEEE Shanghai Section and the 2009–2012 chair of the IEEE Microwave Theory and Techniques Society (MTT-S) Shanghai Chapter. He was the recipient of the National Natural Science Award of China (2004), the National Technology Invention Award of China (2008), and the Best Paper Award of the 2008 Symposium of APEMC in conjunction with the 19th International Symposium of Zurich EMC.

Lijun Jiang (S'01–M'04) received the B.S. degree in electrical engineering from the Beijing University of Aeronautics and Astronautics, Beijing, China, in 1993, the M.S. degree from the Tsinghua University, Beijing, China, in 1996, and the Ph.D. degree from the University of Illinois at Urbana-Champaign, in 2004.

From 1996 to 1999, he was an Application Engineer with the Hewlett-Packard Company. From 2004 to 2009, he was a Postdoctoral Researcher, Research Staff Member, and Senior Engineer with the IBM T. J. Watson Research Center. Since the end of 2009, he has been an Associate Professor with the Department of Electrical and Electronic Engineering, University of Hong Kong, Kowloon, Hong Kong. He was the Semiconductor Research Cooperation (SRC) Industrial Liaison for several academic projects. He serves as a Reviewer of many primary electromagnetics journals and as special sessions organizer for many international conferences. His research interests focus on electromagnetics, EMC/EMI, antennas, multidisciplinary electronic design automation (EDA) solutions, RF and microwave technologies, and high-performance computing (HPC).

Dr. Jiang has been the SRC Packaging High Frequency Topic TT chair since 2009. He has been a Technical Committee member for IEEE EDAPS since 2010. He was a Scientific Committee member of the 2010 IEEE SMEE. He was the guest associate editor of a special issue of the IEEE TRANSACTIONS ON ANTENNAS AND PROPAGATION. He was the recipient of the 1998 HP STAR Award, the 2003 IEEE Microwave Theory and Techniques Society (IEEE MTT-S) Graduate Fellowship Award, the 2004 Y. T. Lo Outstanding Research Award, and the 2008 IBM Research Technical Achievement Award.